

The first Doppler imaging of the active binary prototype RS Canum Venaticorum

Yue Xiang ^{1,2}★, Shenghong Gu,^{1,2,3}★ U. Wolter,⁴ J. H. M. M. Schmitt,⁴
A. Collier Cameron ⁵, J. R. Barnes,⁶ M. Mittag,⁴ V. Perdelwitz ⁴ and S. Kohl⁴

¹Yunnan Observatories, Chinese Academy of Sciences, Kunming 650216, China

²Key Laboratory for the Structure and Evolution of Celestial Objects, Chinese Academy of Sciences, Kunming 650216, China

³University of Chinese Academy of Sciences, Beijing 100049, China

⁴Hamburger Sternwarte, Universität Hamburg, Hamburg 21029, Germany

⁵School of Physics and Astronomy, University of St Andrews, Fife KY16 9SS, UK

⁶Department of Physical Sciences, The Open University, Walton Hall, Milton Keynes MK7 6AA, UK

Accepted 2020 January 7. Received 2020 January 7; in original form 2019 June 21

ABSTRACT

We present the first Doppler images of the prototypical active binary star RS Canum Venaticorum, derived from high-resolution spectra observed in 2004, 2016 and 2017, using three different telescopes and observing sites. We apply the least-squares deconvolution technique to all observed spectra to obtain high signal-to-noise line profiles, which are used to derive the surface images of the active K-type component. Our images show a complex spot pattern on the K star, distributed widely in longitude. All star-spots revealed by our Doppler images are located below a latitude of about 70° . In accordance with previous light-curve modelling studies, we find no indication of a polar spot on the K star. Using Doppler images derived from two consecutive rotational cycles, we estimate a surface differential rotation rate of $\Delta\Omega = -0.039 \pm 0.003 \text{ rad d}^{-1}$ and $\alpha = \Delta\Omega/\Omega_{\text{eq}} = -0.030 \pm 0.002$ for the K star. Given the limited phase coverage during those two rotations, the uncertainty of our differential rotation estimate is presumably higher.

Key words: stars: activity – stars: binaries: eclipsing – stars: imaging – stars: star-spots – stars: individual: RS CVn.

1 INTRODUCTION

RS Canum Venaticorum (CVn)-type stars, as defined by Hall (1976), are a class of close binary systems consisting of a chromospherically active subgiant component, which exhibits brightness variations caused by large cool spots. The prototype star, RS CVn, is an eclipsing binary system composed of an F5 main-sequence star and a K2 subgiant star (Reglero, Giménez & Estela 1990; Rodonò, Lanza & Becciani 2001), with an orbital period of 4.797 695 d (Eaton et al. 1993). Popper (1988) estimated a different spectral type of F4 + G9IV for RS CVn, while Strassmeier & Fekel (1990) determined those two components to be F6IV + G8IV. Barrado et al. (1994) determined the position of the two components on the H–R diagram, which indicated an age of 2.5 Gyr for RS CVn. The mass transfer between two components of RS CVn-type binaries is not relevant for their phenomenology, making them more suitable to study magnetic activity than systems with mass transfer such as Algols.

The distortions in the light curves of RS CVn are attributed to the non-uniformly distributed cool spots (Eaton & Hall 1979; Kang & Wilson 1989). Rodonò, Lanza & Catalano (1995) analysed the long-term sequence photometric data of RS CVn and estimated a period of 19.9 yr for its star-spot activity. They also found a spot migration rate of 0.1° per day during 1963–1984 and a rate of 0.34° per day during 1988–1993, with respect to the rotating frame of the K star. They inferred a solar-like surface differential rotation for the K-type component and the shear rate is about 5–20 per cent of the value of the Sun. Their O – C diagram of the epochs of the primary minima indicates that the orbital period of RS CVn is changing on a time-scale of the order of 100 yr, and the O – C variations are of the order of almost 0.3 d. Such period variations in close binary systems have been proposed to be caused by strong magnetic activity (Applegate 1992). Rodonò et al. (2001) further determined accurate system parameters using a long-term sequence of the light curves of RS CVn, taking into account the light-curve distortions caused by star-spots.

Through analysis of the multi-colour photometry data for RS CVn, Aarum-Ulvås & Henry (2005) found that the hot faculae surrounding cool star-spots on the surface of the cooler component

* E-mail: xy@ynao.ac.cn (YX); shenghonggu@ynao.ac.cn (SG)

were necessary to explain the observed colour variation. Messina (2008) inferred that RS CVn's activity only takes place in the K-type component, and the short-term colour variations are dominated by faculae, whereas the long-term colour variation can be partly caused by the F-type component that makes the system appear bluer when the K component becomes fainter owing to its variable star-spot coverage. From the combination of the photometric and spectroscopic observations of RS CVn, Eaton et al. (1993) found that several moderately sized spots on the surface of the cooler component are needed to fit the observed data. They did not find any evidence for large polar spots.

RS CVn also exhibits signs of magnetic activity in the chromospheric indicators (Fernández-Figueroa et al. 1994; Montes et al. 1996), as well as coronal emission. Its X-ray luminosity of $\log(L_X) = 31.33 \text{ erg s}^{-1}$ (Drake, Simon & Linsky 1992), in combination with the bolometric luminosity derived by Gaia (Gaia Collaboration 2016, 2018), yields $\log(L_X/L_{\text{bol}}) = -3.27$, placing the system close to the saturation limit for late-type main-sequence stars of $\log(L_X/L_{\text{bol}}) = -3$ (Pizzolato et al. 2003).

Up to now, there are only photometric and limited spectroscopic studies on the star-spot activity of this prototype star, and no Doppler image derived for it. The Doppler imaging technique can offer a better constraint on spot latitudes. In order to investigate the spot activities of active binary stars, we continued to monitor a set of RS CVn-type binary systems (Gu et al. 2003; Xiang et al. 2014, 2015, 2016). In this study, we performed high-resolution spectroscopic observations on the active binary prototype RS CVn using three telescopes located at different observing sites. We applied the Doppler imaging code to derive the first detailed spot maps of the K-type component of RS CVn for 2004 February, 2016 January, 2017 April and 2017 November–December.

In Sections 2 and 3, we describe the spectroscopy observations and data reduction. In Section 4, we offer the results of Doppler imaging of the K-type component of RS CVn. We discuss the distribution of star-spots on RS CVn and its surface differential rotation in Section 5. In Section 6, we summarize our results for RS CVn.

2 OBSERVATIONS AND DATA REDUCTION

The high-resolution spectroscopic observations of RS CVn were carried out at three different observing sites, in 2004 February, 2016 January, 2017 April and 2017 November–December. A Coudé echelle spectrograph (CES; Zhao & Li 2001) with a 1024×1024 pixel Tektronix CCD detector mounted on the 2.16 m telescope at the Xinglong station of the National Astronomical Observatories of China was used to collect spectra of RS CVn on 2004 February 3–9. Its resolution power is $R = 37\,000$ and the spectral coverage is 5500–9000 Å. The exposure time varied in a range from 1200–3600 s, depending on the weather. On 2016 January 22–31 and 2017 November 29–December 11, a new fibre-fed high-resolution spectrograph (HRS) with a 4096×4096 pixel EEV CCD detector installed on the 2.16 m telescope at Xinglong station was used to acquire spectral data. It has a resolution power of $R = 48\,000$ and covers from 3900–10000 Å. The exposure time of all these observations was fixed to 1800 s.

A joint observation campaign was carried out by using the 1.2 m robotic spectroscopy telescope, TIGRE (Schmitt et al. 2014), at La Luz Observatory, Guanajuato, Mexico and the 1 m telescope of Shandong University at Weihai on 2017 April 13–21. The TIGRE telescope was equipped with a fibre-fed echelle spectrograph HEROS, which has a resolution power of $R \approx 20\,000$ and a spectral

Table 1. Summary of observations.

Date	Instrument	Resolution	No. of spectra
2004 Feb 3–9	2.16 m/CES	37 000	8
2016 Jan 23–31	2.16 m/HRS	48 000	26
2017 Apr 14–21	TIGRE/HEROS	20 000	46
2017 Apr 18	1 m/HRS	48 000	6
2017 Nov 28–Dec 11	2.16 m/HRS	48 000	29

coverage of 3800–8800 Å with a small gap of 100 Å around 5800 Å. The fibre-fed spectrograph mounted on the 1 m telescope is the same type as the one on the 2.16 m telescope used in 2016 and 2017. Due to bad weather, the 1 m telescope only collected six spectra with sufficient signal-to-noise ratio (SNR), and others are removed to avoid artefacts. We summarize the observations in Table 1, and list them in detail in Appendix A, which is only available online, including UT date, HJD, orbital phase, exposure time and the peak SNR of each observed spectrum.

The spectral data collected with the TIGRE telescope were reduced with the TIGRE data reduction pipeline (Mittag et al. 2010). The data obtained from the 2.16 m and 1 m telescopes were reduced using the IRAF¹ package in a standard way, including image trimming, bias subtraction, flat-field dividing, scatter light subtraction, cosmic ray removal, 1D spectrum extraction, wavelength calibration and continuum fitting. The wavelength calibration was performed by using the comparison spectra of the ThAr lamp taken each night.

3 LEAST-SQUARES DECONVOLUTION

In order to enhance the SNR of the stellar line profiles, we applied the least-squares deconvolution (LSD; Donati et al. 1997) technique to all observed spectra. The LSD technique combines all available observed photospheric lines to derive an average line profile with much higher SNR. The line list, including the central wavelength and depth of spectral lines, was derived from the Vienna Atomic Line Database (VALD; Kupka et al. 1999). In our case, we used the standard LSD technique and only used the line list of the K component in the computation. Tkachenko et al. (2013) showed that using the line list of only one component results in the incorrect depth of the profile of the other component but has little effect on the shapes and the radial velocities of the line profiles of the two stars. We used all available photospheric lines except for those around strong telluric and stellar chromospheric lines to avoid their effects. The SNR of each resulting LSD profile is also listed in Appendix A. The SNR was typically improved by a factor of about 15. For each observing run, we also derived the telluric line profiles from the observed spectra and cross-correlated them to calculate and correct the small instrumental shifts (smaller than 0.5 km s^{-1} for our data sets) that would otherwise introduce errors in the radial velocities and thus improved the Doppler imaging and orbital solutions. This correction method was developed by Collier Cameron (1999) and can achieve a precision better than 0.1 km s^{-1} (Donati et al. 2003).

Our imaging code employs the two-temperature model, which treats the stellar surface as a composition of only two temperature components, the hot photosphere and cool spot, and uses the spot filling factor f to represent the fractional spottedness of each image

¹IRAF is distributed by the National Optical Astronomy Observatory, which is operated by the Association of Universities for Research in Astronomy (AURA) under cooperative agreement with the National Science Foundation.

Table 2. Template stars for the photospheres and spots of two components for each observing site.

Spectra type	TIGRE	Weihai 1 m	Xinglong 2.16 m
F6V	HD 216385	HR 3262	HR 3262
K2IV	HR 5227	HR 5227	HR 8088
M0IV (spot)	HR 4920	HR 4920	HR 4920

pixel (Collier Cameron & Unruh 1994). Thus the spectra of the template stars (Table 2) for the photospheres and star-spots were also deconvolved in the same manner as that for the spectra of RS CVn to construct the lookup tables, which contain the local intensity profiles of two temperature components at different limb angles on the stellar surface. We obtained the linear limb-darkening coefficients of UBVRI passbands from Claret, Hauschildt & Witte (2012, 2013), for the effective temperatures of the photospheres and spots of the F main-sequence and K subgiant stars. The spot temperature of 3500 K was chosen according to the values of similar systems. Given the fact that the limb-darkening coefficient is almost a linear function of the wavelength, for each temperature component of each star we used a linear interpolation to derive the value at the centroidal wavelength of 6170 Å, which was calculated from the line list (Barnes et al. 1998). The results are 0.84 and 0.77 for the star-spot and photosphere of the K star, and 0.76 and 0.55 for those of the F star, respectively. Then we calculated the local intensity at 30 limb angles to produce the lookup tables.

4 DOPPLER IMAGING

4.1 System parameters

The Doppler imaging technique requires accurate stellar parameters, such as the projected rotational velocity ($v \sin i$), inclination and rotational period, to derive reliable surface maps and to prevent the production of artefacts (Collier Cameron & Unruh 1994), especially for eclipsing binary systems (Vincent, Piskunov & Tuominen 1993). It has been demonstrated that the Doppler imaging code can also be used to determine the stellar parameters of single and binary stars (e.g. Barnes et al. 1998, 2004). Fine-tuning stellar parameters can be achieved by performing a fixed number of maximum entropy iterations with various combinations of stellar parameters and then finding the best-fitting values that lead to a minimum χ^2 . This method can overcome the effect of star-spot distortions on the parameter determinations (Barnes et al. 2005a).

In this work, we performed the χ^2 minimization method to estimate the best stellar parameters for Doppler imaging of RS CVn. Since the orbital elements of RS CVn have been widely studied (e.g. Catalano & Rodonò 1974; Popper 1988; Eaton et al. 1993), we adopted the values of the inclination (i), the orbital period (P_{orbit}) and conjunction time (T_0) derived by Eaton et al. (1993) and the albedo coefficients of the two stars in the paper of Rodonò et al. (2001) as fixed parameters that did not change in the procedure. We used the values of the mass ratio (q), the radial velocity amplitudes of the two stars (K) derived by Eaton et al. (1993) as the initial guess, and performed a grid search within a small range around them to search for the best-fitting values. With a small systematic orbital phase offset in a range of 0.0007–0.0019 for each observing run, which takes the long-term orbital period variation into account, we found that the orbital ephemeris taken from Eaton et al. (1993) is sufficient for Doppler imaging. We show the deviation of orbital phase and the corresponding conjunction time between the values calculated from

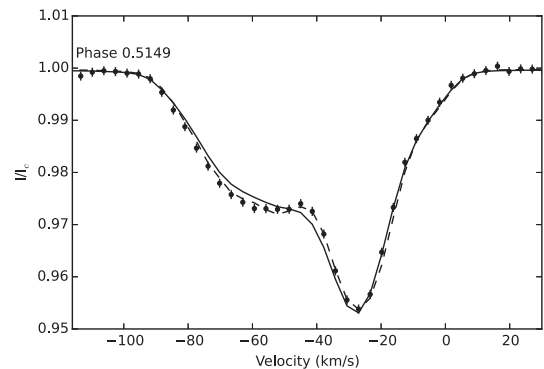
Table 3. Deviation of orbital phase and the corresponding ΔT_0 between the values calculated from our data sets and those from the ephemeris of Eaton et al. (1993).

Epoch (mean HJD) + 245 0000	$\Delta\phi$ O – C	ΔT_0 O – C (d)
3042.5	−0.0011	0.0052
7415.4	−0.0019	0.0091
7861.9	−0.0007	0.0034
8094.0	−0.0013	0.0062

Table 4. Adopted stellar parameters of RS CVn for Doppler imaging.

Parameter	Value	Ref.
$q = M_K/M_F$	1.07 ± 0.01	DoTS
K_F (km s $^{-1}$)	90.2 ± 0.1	DoTS
K_K (km s $^{-1}$)	84.3	K_F and q
i (°)	85.55	a
T_0 (HJD)	244 8379.1993	a
P_{orbit} (d)	4.797 695	a
$v \sin i_F$ (km s $^{-1}$)	12.4 ± 0.5	DoTS
$v \sin i_K$ (km s $^{-1}$)	44.9 ± 1.0	DoTS
R_F (R_\odot)	2.1	DoTS
R_K (R_\odot)	4.3	DoTS
$P_{\text{rot},F}$ (d)	8.542	$v \sin i$, i and R_F
$T_{\text{eff},F}$ (K)	6800	a
$T_{\text{eff},K}$ (K)	4580	a
Albedo $_F$	1.0	b
Albedo $_K$	0.3	b

Note. References: a. Eaton et al. (1993); b. Rodonò et al. (2001).


Figure 1. A comparison of the fits to the LSD profile observed at eclipsing phase 0.5149 with 2.16 m/HRS, assuming synchronous (solid line) or non-synchronous rotation (dashed line) of the F component.

our data sets and those from the ephemeris of Eaton et al. (1993) in Table 3. We list the adopted values of the stellar parameters for imaging RS CVn in Table 4.

In the imaging process, we noticed that we cannot obtain a good fit with the assumption of synchronous rotation. The F-type component seems to have a significantly smaller rotational speed, similar to another RS CVn-type system, SZ Psc (Xiang et al. 2016). As an example, Fig. 1 shows the fit to the observed LSD profile at phase 0.5149, where the F star was eclipsing the K star. The misfit is obvious if our imaging code treats it as a synchronous binary system. Given a $v \sin i$ of 12.4 km s $^{-1}$ derived from line profile broadening,

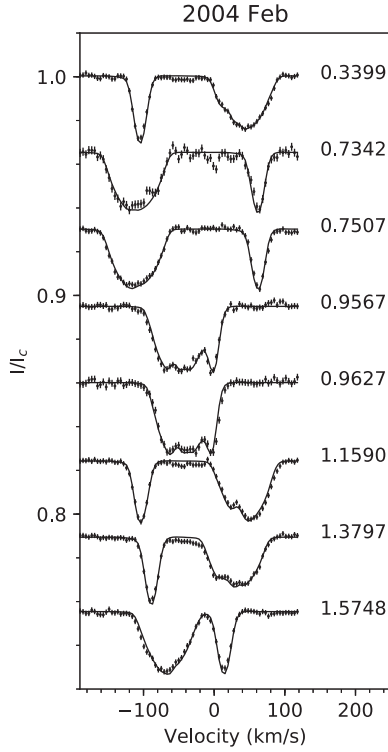


Figure 2. Doppler imaging line profile fits (lines) and data set (dots with 1σ error bars) collected by 2.16 m/CES in 2004 February. The rotational cycles are marked beside each profile. The reduced $\chi^2 = 1.41$.

the radius of the F star is only $1.2 R_{\odot}$ assuming that it is tidally locked. By contrast, Eaton et al. (1993) derived a stellar radius of about $2.0 R_{\odot}$ for the F star from the light-curve modelling. Strassmeier & Fekel (1990) and Eaton et al. (1993) found that the difference between the widths of the observed and calculated profiles for the F star can be attributed to the non-synchronous rotation.

To deal with it, we have a minor modification on the Doppler imaging code to take into account the non-synchronous rotation of the F-type component. This is achieved by recalculating the positions of the stellar grids and the velocity of pixels in the view plane when integrating the flux of the F star, according to its rotational rate and stellar radius. The detailed modification method was described in our previous paper (Xiang et al. 2016). As a result, we found that the F star rotates about 1.8 times more slowly than expected on the basis of synchronous rotation. The projected rotational velocity of the F star is $v \sin i = 12.4 \text{ km s}^{-1}$, whereas the synchronous rotation velocity derived from the orbital period and the stellar radius is $v \sin i = 22.3 \text{ km s}^{-1}$. Our result is consistent with that of Strassmeier & Fekel (1990). Their estimates of the rotation rates of the F and K stars are $11 \pm 2 \text{ km s}^{-1}$ and $42 \pm 3 \text{ km s}^{-1}$, respectively.

4.2 Spot images

We used the imaging code Doppler Tomography of Stars (DOTS; Collier Cameron 1992; Collier Cameron 1997) to implement the maximum entropy regularized iterations to all of the data sets. Figs 2–5 show the maximum entropy fits to the observed LSD profiles of the data sets in 2004 February, 2016 January, 2017 April

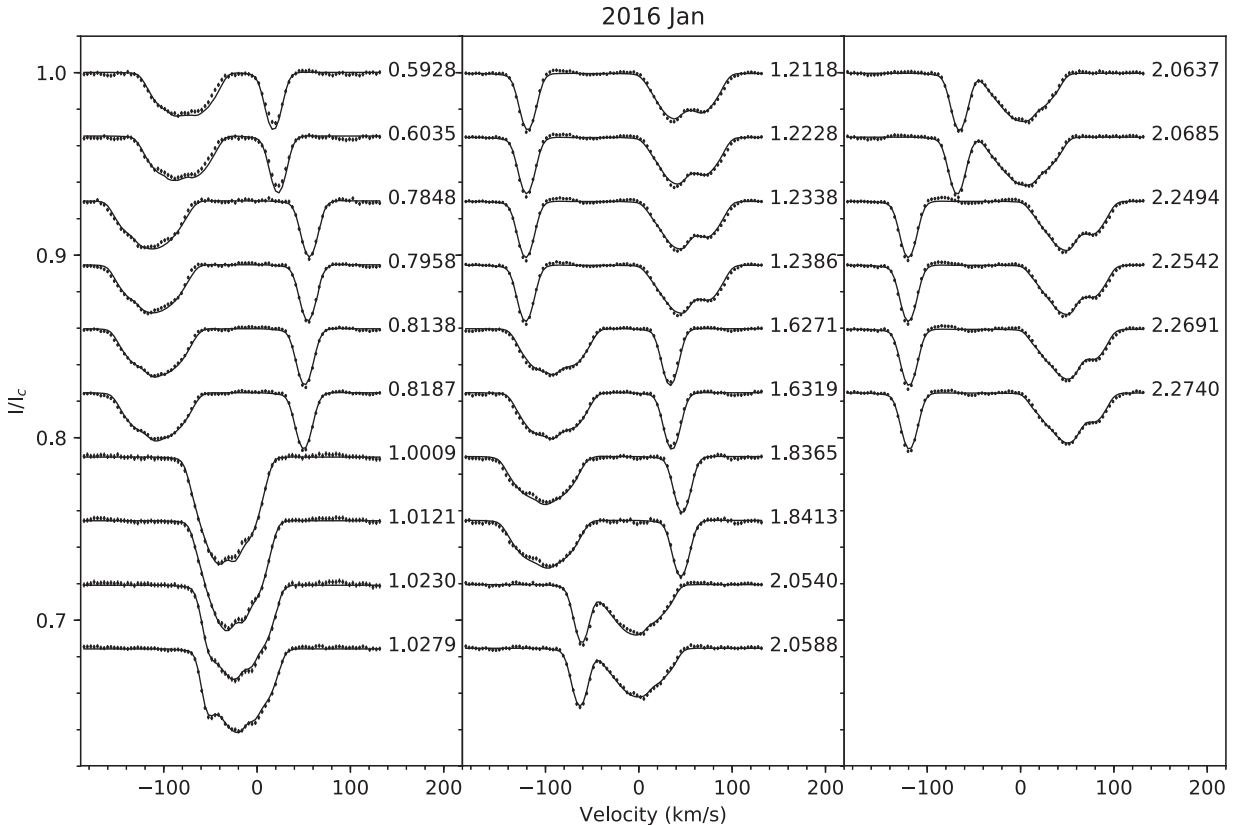


Figure 3. Same as Fig. 2, but for the data set collected by 2.16 m/HRS in 2016 January. The reduced $\chi^2 = 1.29$.

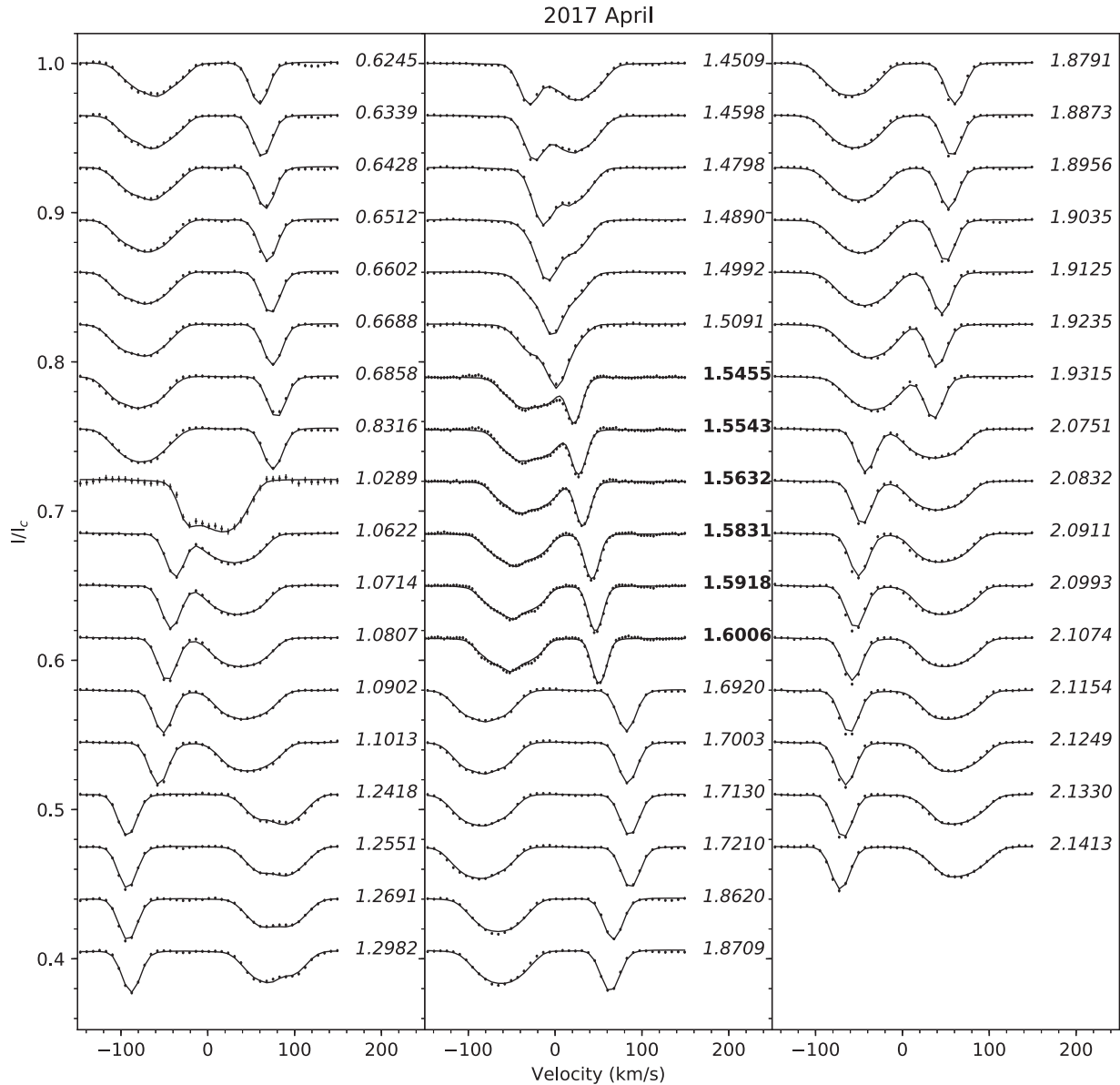


Figure 4. Same as Fig. 2, but for the data sets collected by TIGRE/HEROS (phases in italics) and 1 m/HRS (phases in bold) in 2017 April. The reduced $\chi^2 = 1.07$.

and 2017 November–December. The reduced χ^2 for each data set is shown in the caption of each figure. We did not achieve a reduced χ^2 of 1.0, due to the underestimated errors in the LSD computation (Donati et al. 1997; Barnes et al. 2005a) and the maximum entropy regularization. Fig. 6 shows the reconstructed images of the K-type component of RS CVn derived from these four data sets. The mean spot filling factor as a function of latitude is also plotted for each image. Given the $v \sin i$ of the K star of RS CVn and the resolution power of the spectrograph, the data sets collected by 2.16 m/CES, 2.16 m/HRS, 1 m/HRS and TIGRE/HEROS, respectively, offered about 12, 15, 15, 6 resolution elements across the stellar disc, which translate into longitudinal resolutions of about 15° , 12° , 12° and 30° , respectively, for the Doppler imaging (Borisova et al. 2019).

In our spot maps, phase 0.5 (longitude 180°) on the K-type component faces the F-type component. One should notice an obvious spurious feature in all of the Doppler images that the low-

latitude spots are smeared and elongated vertically. This is due to the poor latitude resolution of the Doppler imaging technique for low-latitude features. Hence the shapes of the low-latitude spots should not be over-interpreted. The mirroring effect is strong for high inclination stars like RS CVn, but can be broken by the eclipse (Vincent et al. 1993). The spots in the images of the K star of 2017 April and November–December show sharp edges around phase 0.5 due to the passage of the F star.

The surface image of 2004 February shows connected structures between phases 0.2 and 0.6, composed of several spots. The features extend from latitude 0° to 60° . Two connected spots appear at the stellar equator around phase 0.95. The image of 2016 January shows several spot groups at phases 0, 0.2, 0.4, 0.6, 0.9. A strong spot is located at latitude 45° and phase 0.2 with appendages extending to the stellar equator.

The 2017 April data set has the best phase coverage among the four observing runs. The image shows strong spots at the equator

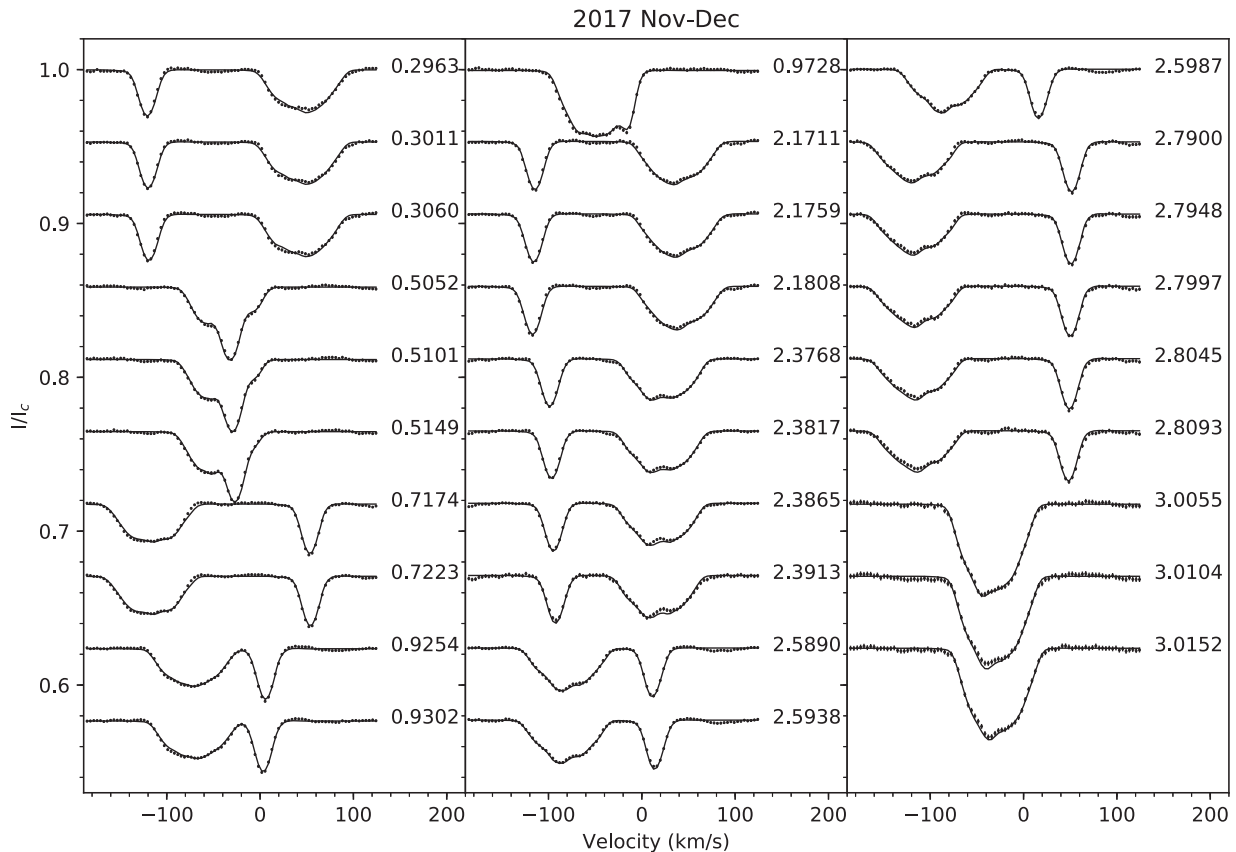


Figure 5. Same as Fig. 2, but for the data set collected by 2.16 m/HRS in 2017 November–December. The reduced $\chi^2 = 1.26$.

around phases 0.3 and 0.5, and a spot at latitude 30° and phase 0.7. These spots are also appended by weak spot features. The image derived for 2017 November–December, which is about half a year apart from the 2017 April observing run, shows a similar spot pattern. However, the latitudinal concentration of the spot activity changed from 10° to 50° , as seen in the mean spot filling factor versus latitude plot. The spot at phase 0.3 in 2017 April disappeared in 2017 November–December, while a strong spot emerged at phase 0.4 latitude 60° . The region around phase 0.5 was still active, and the spot group around phase 0.7 seemed to be retained, but its position and distribution changed.

We also present images of the binary system at orbital phases 0, 0.25, 0.5 and 0.75 of one orbital cycle in Fig. 7, using the Doppler images of 2017 April. Since the rotational velocity of the F star is too slow (Table 4), its reconstructed surface features are mainly related to the changes of the LSD line strength, and may not represent actual features on the F star’s surface.

The Doppler image for 2017 April was derived from a combined data set collected by two telescopes, the 1.2 m TIGRE telescope and Weihai 1 m telescope, at different observing sites in the same epoch to obtain a better phase sampling. However, the spectral resolution of the two instruments differs by a factor of about 2.5, as described in Section 2. To show the effect of different spectral resolutions on the image, we also derived a spot map from the data set acquired by the TIGRE telescope only, as shown in the lower panel in Fig. 8. Since the Weihai data set only covered phases 0.5455–0.6006, we cannot use it to derive an image independently. As seen in Fig. 8, the spot patterns of the two images are very similar to each other, but the data set from the Weihai 1 m telescope helps to uncover finer spot structures, especially for phases 0.4–0.7. The spot image

derived only from the TIGRE data set shows an unresolved feature at phase 0.6, but the image from the combined spectra reveals that it is a connected structure of two smaller spots. One is a spot at phase 0.6 and the other is a weaker feature at phase 0.7. This also hints that there should be more smaller spots on the surface of the K subgiant component of RS CVn, which are not resolved due to the limited spectral resolution.

4.3 Surface differential rotation

Star-spots are the tracers of stellar surface rotation, and the comparison between the Doppler images observed within several rotational cycles can reveal surface differential rotation patterns. The shear rate can be estimated either by the cross-correlation of two maps observed in close epochs (Donati & Collier Cameron 1997) or by the shear imaging method, which takes the differential rotation rate as a parameter directly in the Doppler imaging process (Petit, Donati & Collier Cameron 2002). Here we apply the cross-correlating map method to estimate the surface differential rotation rate for the K star of RS CVn.

The spot configurations of two Doppler images will be biased if the phase coverage is incomplete and different. Hence we only chose the 2016 January data set to estimate the differential rotation rate, since it covered two consecutive rotation cycles with very similar phase coverage to each other. We partitioned the spectra of this data set into two subsets covering the rotation cycles 0.59–1.24 and 1.63–2.27, respectively. Then we separately derived two Doppler images from these two subsets, as shown in the upper two panels of Fig. 9. The cross-correlation function between the two Doppler images, excluding the large phase gap of 0.30–0.55, was calculated

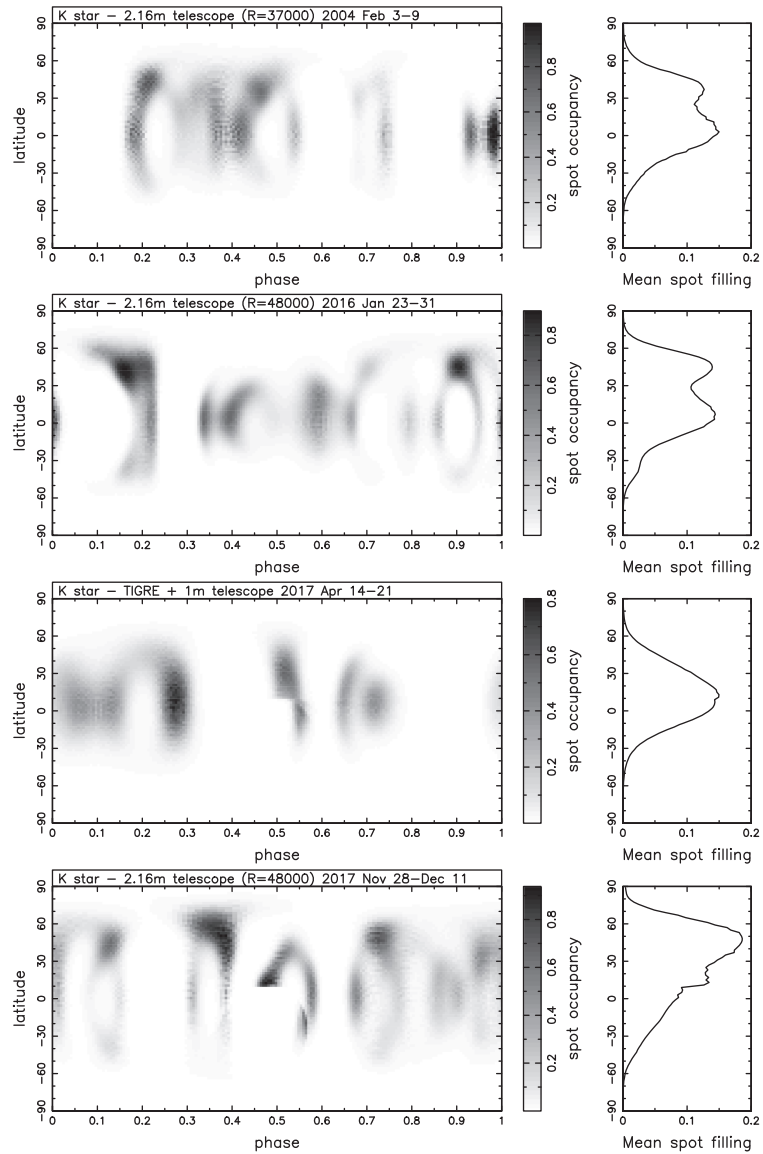


Figure 6. Doppler images of the K star for 2004 February, 2016 January, 2017 April, 2017 November–December. The observed phases are marked by vertical ticks. The mean spot filling factor versus latitude is plotted beside each image. The equatorial spots at phase 0.5 show sharp edges due to the passage of the F star.

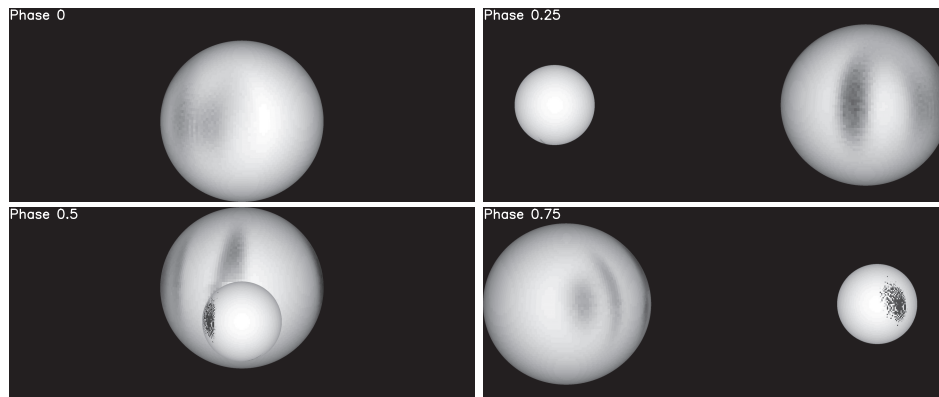


Figure 7. Images of the binary system at orbital phases 0, 0.25, 0.5 and 0.75 in 2017 April. Due to the very slow rotation speed of the F star, the spot features on its surface are probably artefacts.

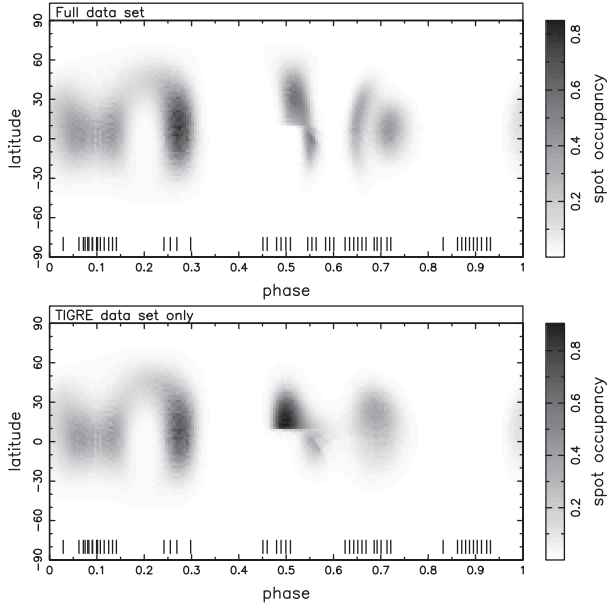


Figure 8. Comparison of the Doppler images derived from the combined TIGRE and Weihai data sets and the TIGRE data set only. The images are consistent where the two data sets overlap, and the Weihai data set has a larger resolution.

latitude by latitude. The resulting cross-correlating map is shown as a greyscale plot in the bottom panel of Fig. 9. Then we fitted the peak phase shift of the cross-correlation function of each latitude belt between 10° and 60° (Fig. 9), since the high-latitude regions are featureless and the Doppler imaging is insensitive to the latitude of the equatorial spots. We assumed a solar-like latitude-dependent surface rotation law as

$$\Omega(l) = \Omega_{\text{eq}} - \Delta\Omega \sin^2 l \quad (1)$$

where Ω_{eq} is the angular velocity rate at the stellar equator, l is the latitude and $\Delta\Omega$ is the difference between the rotation rates at the stellar equator and the pole. The results show that the surface rotation law for the K-type component of RS CVn follows $\Omega(l) = 1.293(\pm 0.001) + 0.039(\pm 0.003)\sin^2 l$ [rad d $^{-1}$]. However, due to the limited number of mid-to-high latitude spots, poor phase coverage and spot evolution, the error is presumably underestimated.

5 DISCUSSION

We have presented maximum entropy reconstructed images of the active binary prototype RS CVn for 2004 February, 2016 January, 2017 April and 2017 November–December, derived from high-resolution spectra collected with three telescopes at different observing sites. The K-type component of RS CVn exhibited star-spot activity in all four observing seasons. The surface images indicate complex spot patterns on the surface of the K star, which showed many small-to-moderate star-spots, instead of one or two large active regions. The spot configurations revealed by our Doppler images are in excellent agreement with the results of Eaton et al. (1993). They found that six to eight moderately sized spots on the surface of the K-type component are necessary for fitting the spectral line profiles of RS CVn. For the observed light curves, they also demonstrated that the multi-spot solution is better than the three-spot solution.

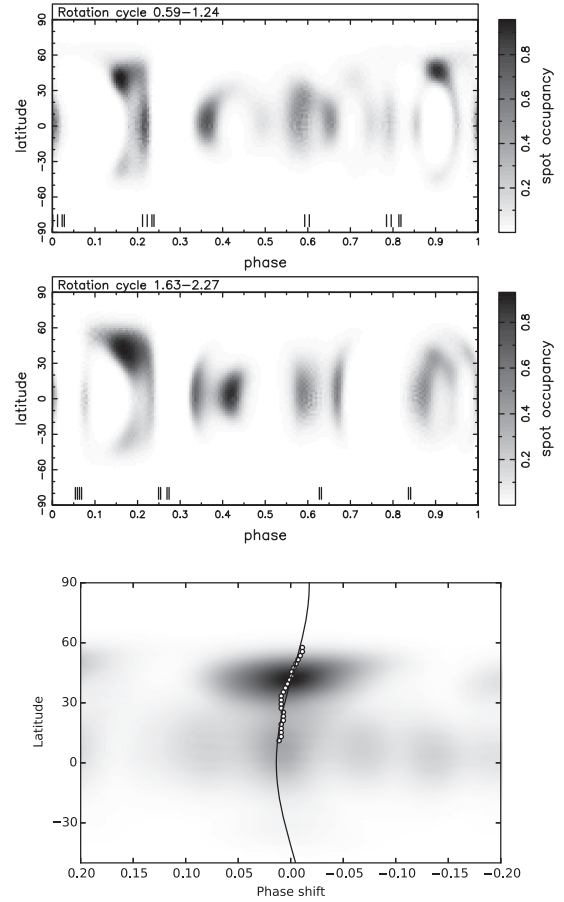


Figure 9. The upper two panels show images derived from two consecutive rotation cycles. The bottom panel shows a cross-correlating map for these two images. The maximum values of the cross-correlation function at each latitude belt between latitudes 0° and 60° are marked as open circles, and a curve is fitted with equation (1) given in Section 4.3. Note that the x -axis of the cross-correlation map is inverse, since a negative phase shift means a shorter rotation period and faster rotation speed.

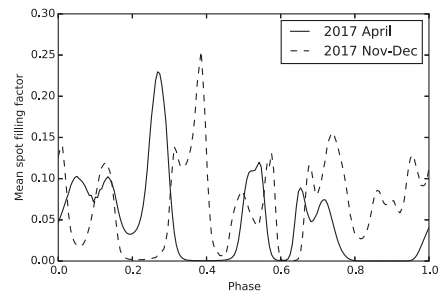


Figure 10. Mean spot filling factor as a function of longitude for 2017 April and 2017 November–December.

The Doppler images also indicate a non-uniform longitudinal distribution of the star-spots on the K star. In each observing season, we detected several active longitudes. We plot the mean spot filling factors as functions of longitude, for the 2017 April and 2017 November–December images, in Fig. 10. The K star showed four active longitudes in 2017 April, but exhibited one more active region around phase 0.9 in 2017 November–December. The cross-correlation of two longitudinal distributions of mean spot filling factor between phases 0.1 and 0.8, where the common

active longitudes existed, indicates a systematic phase shift of 0.08. Theoretically, the preferred longitudes may be produced by a non-axisymmetric dynamo (Moss, Piskunov & Sokoloff 2002). For close binaries, the tidal force also plays an important role in the formation of active longitudes, since it can effectively affect the arising flux-tubes (Holzwarth & Schüssler 2003). Active longitude migrations on the K star have been observed by many authors through long-term light-curve modelling (Eaton, Hall & Henry 1980; Kang & Wilson 1989; Heckert & Ordway 1995). They respectively revealed migration periods of 9.48 yr, 9.4 yr and 8.8 yr for the active region. Rodonò et al. (1995) detected up to three active longitudes on the K star of RS CVn and found their migration rates to be 0.1° per day in the direction of the rotation during 1963–1984 and 0.34° per day during 1988–1993. They attributed this to being a result of the solar-like differential rotation on the surface of the K star. Comparing our spot maps of the K star in 2017 April and 2017 November–December, the systematic drift of 0.08 in phase, corresponding to -30° in longitude, may indicate a migration rate of 0.14° per day, but in the opposite direction of the stellar rotation, during the time interval of our two observing runs. However, apparently we cannot confirm this with the current data, since these two data sets were obtained 220 d apart and the spots may evolve greatly during this time span. Eaton & Hall (1979) found that the star-spots on the K star have lifetimes of less than one year, but Heckert & Ordway (1995) observed star-spot lifetimes in a range between 2 and 6 yr.

Another notable feature is the latitude distribution of the star-spots on the K star. Our Doppler images indicate that all spots were located below latitude 70° , and we did not find any high-latitude feature or polar cap in any of the four observing seasons. The lack of polar spots revealed by our Doppler images is very consistent with previous studies. Rodonò et al. (1995) demonstrated that no polar spot is required to fit their long-term light curves within the observation errors. Eaton et al. (1993) revealed that there is no evidence for sizeable polar spots on the K star. From their observed line profiles, they even suspected it to have polar star-spots smaller than 18° in radius.

The absence of high-latitude features on the K-type subgiant component of the prototype RS CVn is interesting, considering its relatively high rotational velocity ($v \sin i = 44.9 \text{ km s}^{-1}$). High-latitude spots and long-lived polar caps are commonly found on the surface of the rapidly rotating active components of RS CVn-type binary systems, revealed by both photometric and spectroscopic studies. Several active single rapid rotators, such as AB Dor (Collier Cameron & Unruh 1994) and FK Com-type stars (Strassmeier et al. 1999), were also reported to have large polar active regions. In our previous works, we found persistent high-latitude or polar features on active binaries with various rotational speeds, such as II Peg ($v \sin i = 22 \text{ km s}^{-1}$; Xiang et al. 2014), SZ Psc ($v \sin i = 67.7 \text{ km s}^{-1}$; Xiang et al. 2016) and ER Vul ($v \sin i = 80 \text{ km s}^{-1}$; Xiang et al. 2015).

Theoretical models suggest that the dominant Coriolis force and the meridional circulation can affect the magnetic flux transport within the convection zone to produce high-latitude magnetic emergence, and thus the latitude distribution of star-spots is dependent on the rotational speed and the thickness of the convection zone (Schüssler et al. 1996; Mackay et al. 2004; Holzwarth, Mackay & Jardine 2006). Flux-tubes that emerge at low latitude can also be advected polewards by surface flows (Işık, Schüssler & Solanki 2007; Işık, Schmitt & Schüssler 2011). For the lack of high-latitude spots on the Sun, Schüssler & Solanki (1992) offered a simple scenario that the magnetic field at the bottom of the convection zone is 10 times larger than the equipartition field strength, which results in the dominant buoyancy force. However, the tidal force and higher

rotational speed make the dynamo process in close binaries more complex than that for single stars. An estimate from Paternò et al. (2002) shows that the ratio of toroidal to poloidal magnetic fields of RS CVn is less than 10 per cent that of the Sun, which implies that it is dominated by an α^2 - Ω dynamo regime rather than an α - Ω one.

The surface differential rotation is an important factor in the stellar dynamo process. The cross-correlation of our Doppler images indicates an anti-solar surface shear rate of $\Delta\Omega = -0.039 \pm 0.003 \text{ rad d}^{-1}$ and $\alpha = \Delta\Omega/\Omega_{\text{eq}} = -0.030 \pm 0.002$ for the K star of RS CVn, which means that the pole of the K subgiant rotates faster than the equator and laps it once every 161 d. Evidence for the surface latitudinal differential rotation of RS CVn was also found by Rodonò et al. (1995), but they inferred a solar-like shear rate of $\Delta\Omega = 2.3^\circ \pm 1.6^\circ \text{ d}^{-1}$ ($0.0401 \pm 0.0279 \text{ rad d}^{-1}$) to explain the spot migrations found in the light-curve analysis. Our estimate of the differential rotation rate was based on only two Doppler images. The phase coverage was not ideal and the value of shear rate is almost exclusively dependent on the large spot structure at phase 0.2. Meanwhile, the evolution of star-spots also induces errors in the estimate of the differential rotation rate. More observations are required to confirm the differential rotation of the K-type star.

Recent Doppler imaging studies have detected solar-like surface differential rotation on both single and binary stars (Barnes et al. 2000; Dunstone et al. 2008; Kriskovics et al. 2014; Özdarcın et al. 2016), while some close binaries have been reported to show anti-solar differential rotations, which may be attributed to the tidal force (Kővári et al. 2015; Harutyunyan et al. 2016). Gastine et al. (2014), Brun et al. (2017) showed that the different directions of the differential rotations are related to the predominance of the Coriolis force over the buoyancy force and vice versa. Barnes et al. (2005b) analysed the differential rotation rates of 10 stars determined by the Doppler imaging technique, and revealed that the shear rate decreases with decreasing effective temperature. Kővári et al. (2017) further investigated differential rotation of single and binary stars, and revealed that the trends of the surface shear rate of single stars are significantly different to those of close binaries, whose differential rotation is confined by the tidal force.

6 CONCLUSION

We have presented the first Doppler images of the active K-type subgiant component of the prototype RS CVn, derived from four data sets observed from 2004 to 2017. Based on the new reconstructed images, we summarize the results as follows.

1. The K-type component of RS CVn shows spot activity in all observing seasons. The Doppler images reveal complex spot patterns on the K star, which exhibits several small-to-moderate star-spots.
2. The reconstructed images indicate that all spots are located below latitude 70° , and we do not find any high-latitude or polar spots.
3. The K star shows a non-uniform longitudinal spot distribution. We find several active longitudes on its surface and clues for spot migrations.
4. Using the cross-correlating technique, we derive an anti-solar differential rotation rate of $\Delta\Omega = -0.039 \pm 0.003 \text{ rad d}^{-1}$ and $\alpha = \Delta\Omega/\Omega_{\text{eq}} = -0.030 \pm 0.002$ for the K-type component of RS CVn. Due to the limited phase coverage and the evolution of spot patterns, the uncertainty of our differential rotation estimate is presumably higher.

In the future, more observations with shorter intervals and longer time baselines are required to reveal the short-term evolution of star-

spots and the surface differential rotation on the K-type component of the active binary RS CVn.

ACKNOWLEDGEMENTS

This work is supported by the National Natural Science Foundation of China through grants No. 10373023, No. 11333006 and No. 11603068. The joint research project between Yunnan Observatories and Hamburg Observatory is funded by the Sino-German Center for Research Promotion (GZ1419). UW acknowledges funding by DLR, project 50OR1701. We would like to thank Prof. Jianyan Wei and Prof. Xiaojun Jiang for the allocation of observing time for the Xinglong 2.16 m telescope. We are very grateful to the anonymous referee for helpful comments and suggestions that significantly improved the clarity and quality of this paper. This work is based on data obtained with the TIGRE telescope, located at La Luz observatory, Mexico. TIGRE is a collaboration of the Hamburger Sternwarte, the Universities of Hamburg, Guanajuato and Liège. This work has made use of the VALD database, operated at Uppsala University, the Institute of Astronomy RAS in Moscow, and the University of Vienna.

REFERENCES

Aarum-Ulvås V., Henry G. W., 2005, *Astron. Nachrichten*, 326, 292
 Applegate J. H., 1992, *ApJ*, 385, 621
 Barnes J. R., Collier Cameron A., Unruh Y. C., Donati J.-F., Hussain G. A. J., 1998, *MNRAS*, 299, 904
 Barnes J. R., Collier Cameron A., James D. J., Donati J.-F., 2000, *MNRAS*, 314, 162
 Barnes J. R., Lister T. A., Hilditch R. W., Collier Cameron A., 2004, *MNRAS*, 348, 1321
 Barnes J. R., Collier Cameron A., Lister T. A., Pointer G. R., Still M. D., 2005a, *MNRAS*, 356, 1501
 Barnes J. R., Collier Cameron A., Donati J.-F., James D. J., Marsden S. C., Petit P., 2005b, *MNRAS*, 357, L1
 Barrado D., Fernández-Figueroa M. J., Montesinos B., De Castro E., 1994, *A&A*, 290, 137
 Borisova A., Wolter U., Konstantinova-Antova R., Schröder K. P., 2019, *Bulgarian Astron. J.*, 31, 76
 Brun A. S. et al., 1979, *ApJ*, 836, 192
 Catalano S., Rodonò M., 1974, *PASP*, 86, 390
 Claret A., Hauschildt P. H., Witte S., 2012, *A&A*, 546, A14
 Claret A., Hauschildt P. H., Witte S., 2013, *A&A*, 552, A16
 Collier Cameron A., 1992, in Byrne P., Mullan D., eds, *Lecture Notes in Physics*, Vol. 397, *Surface Inhomogeneities on Late-Type Stars*. Springer, Berlin, p. 33
 Collier Cameron A., 1997, *MNRAS*, 287, 556
 Collier Cameron A., 1999, in Hearnshaw J. B., Scarfe C. D., eds, *ASP Conf. Ser. Vol. 185, Precise Stellar Radial Velocity*. Astron. Soc. Pac., San Francisco, p. 233
 Collier Cameron A., Unruh Y. C., 1994, *MNRAS*, 269, 814
 Donati J.-F., Collier Cameron A., 1997, *MNRAS*, 291, 1
 Donati J.-F., Semel M., Carter B. D., Rees D. E., Collier Cameron A., 1997, *MNRAS*, 291, 658
 Donati J.-F. et al., 2003, *MNRAS*, 345, 1145
 Drake S. A., Simon T., Linsky J. L., 1992, *ApJS*, 82, 311
 Dunstone N. J., Hussain G. A. J., Collier Cameron A., Marsden S. C., Jardine M., Barnes J. R., Ramirez Velez J. C., Donati J.-F., 2008, *MNRAS*, 387, 1525
 Eaton J. A., Hall D. S., 1979, *ApJ*, 227, 907
 Eaton J. A., Hall D. S., Henry G. W., 1980, *IBVS*, No. 1862
 Eaton J. A., Henry G. W., Bell C., Okorogu A., 1993, *AJ*, 106, 1181
 Fernández-Figueroa M. J., Montes D., De Castro E., Cornide M., 1994, *ApJS*, 90, 433
 Gaia Collaboration, 2016, *A&A*, 595, A1
 Gaia Collaboration, 2018, *A&A*, 616, A1

Gastin T., Yadav R. K., Morin J., Reiners A., Wicht J., 2014, *MNRAS*, 438, L76
 Gu S.-H., Tan H.-S., Wang X.-B., Shan H.-G., 2003, *A&A*, 405, 763
 Hall D. S., 1976, in Fitch W. S., ed., *Proc. IAU Colloq. 29, Multiple Periodic Variable Stars*. Reidel, Dordrecht, p. 287
 Harutyunyan G., Strassmeier K. G., Künstler A., Carroll T. A., Weber M., 2016, *A&A*, 592, A117
 Heckert P. A., Ordway J. I., 1995, *AJ*, 109, 2169
 Holzwarth V., Schüssler M., 2003, *A&A*, 405, 303
 Holzwarth V., Mackay D. H., Jardine M., 2006, *MNRAS*, 369, 1703
 Işık E., Schüssler M., Solanki S. K., 2007, *A&A*, 464, 1049
 Işık E., Schmitt D., Schüssler M., 2011, *A&A*, 528, A135
 Kang Y. W., Wilson R. E., 1989, *AJ*, 97, 848
 Kővári Zs. et al., 2015, *A&A*, 573, A98
 Kővári Zs., Oláh K., Kriskovics L., Vida K., Forgács-Dajka E., Strassmeier K. G., 2017, *Astron. Nachrichten*, 338, 903
 Kriskovics L., Kővári Zs., Vida K., Granzer T., Oláh K., 2014, *A&A*, 571, A74
 Kupka F., Piskunov N., Ryabchikova T. A., Stempels H. C., Weiss W. W., 1999, *A&AS*, 138, 119
 Mackay D. H., Jardine M., Collier Cameron A., Donati J. F., Hussain G. A. J., 2004, *MNRAS*, 354, 737
 Messina S., 2008, *A&A*, 480, 495
 Mittag M., Hempelmann A., González-Pérez J. N., Schmitt J. H. M. M., 2010, *Advances Astron.*, 2010, 101502
 Montes D., Fernández-Figueroa M. J., Cornide M., De Castro E., 1996, *A&A*, 312, 221
 Moss D., Piskunov N., Sokoloff D., 2002, *A&A*, 396, 885
 Özdarcan O., Carroll T. A., Künstler A., Strassmeier K. G., Evren S., Weber M., Granzer T., 2016, *A&A*, 593, A123
 Paternò L., Belvedere G., Kuzanyan K. M., Lanza A. F., 2002, *MNRAS*, 336, 291
 Petit P., Donati J.-F., Collier Cameron A., 2002, *MNRAS*, 334, 374
 Pizzoloto N., Maggio A., Micela G., Sciortino S., Ventura P., 2003, *A&A*, 397, 147
 Popper D. M., 1988, *AJ*, 95, 1242
 Reglero V., Giménez A., Estela A., 1990, *A&A*, 231, 375
 Rodonò M., Lanza A. F., Catalano S., 1995, *A&A*, 301, 75
 Rodonò M., Lanza A. F., Becciani U., 2001, *A&A*, 371, 174
 Schmitt J. H. M. M. et al., 2014, *Astron. Nachrichten*, 335, 787
 Schüssler M., Solanki S. K., 1992, *A&A*, 264, L13
 Schüssler M., Caligari P., Ferriz-Mas A., Solanki S. K., Stix M., 1996, *A&A*, 314, 503
 Strassmeier K. G., Fekel F. C., 1990, *A&A*, 230, 389
 Strassmeier K. G., Lupinek S., Dempsey R. C., Rice J. B., 1999, *A&A*, 347, 212
 Tkachenko A., Van Reeth T., Tsymbal V., Aerts C., Kochukhov O., Debusscher J., 2013, *A&A*, 560, A37
 Vincent A., Piskunov N. E., Tuominen I., 1993, *A&A*, 278, 523
 Xiang Y., Gu S.-H., Collier Cameron A., Barnes J. R., 2014, *MNRAS*, 438, 2307
 Xiang Y., Gu S.-H., Collier Cameron A., Barnes J. R., 2015, *MNRAS*, 447, 567
 Xiang Y., Gu S.-H., Collier Cameron A., Barnes J. R., Zhang L. Y., 2016, *MNRAS*, 456, 314
 Zhao G., Li H.-B., 2001, *Chinese J. Astron. Astrophys.*, 1, 555

SUPPORTING INFORMATION

Supplementary data are available at *MNRAS* online.

APPENDIX A: OBSERVING LOG

Please note: Oxford University Press is not responsible for the content or functionality of any supporting materials supplied by the authors. Any queries (other than missing material) should be directed to the corresponding author for the article.

This paper has been typeset from a $\text{\TeX}/\text{\LaTeX}$ file prepared by the author.